

# Softening and melting mechanisms of polyamides interfering with sliding stability under adhesive conditions

P. Samyn<sup>a,\*</sup>, G. Schoukens<sup>b</sup>, I. Van Driessche<sup>c</sup>, J. Van Craenenbroeck<sup>c</sup>, F. Verpoort<sup>c</sup>

<sup>a</sup> *Laboratory Soete, Department of Mechanical Construction and Production, Ghent University, Sint-Pietersnieuwstraat 41, B-9000 Gent, Belgium*

<sup>b</sup> *Department of Textiles, Ghent University, Technologiepark 907, B-9052 Zwijnaarde, Belgium*

<sup>c</sup> *Laboratory of Organometallics and Catalysis, Department of Inorganic and Physical Chemistry, Ghent University, Krijgslaan 281 (S3), B-9000 Gent, Belgium*

Received 7 February 2006; received in revised form 22 March 2006; accepted 12 May 2006

Available online 2 June 2006

## Abstract

The thermal stability of polymers is a main issue when used as friction elements under dry sliding. Cast polyamide grades processed with either sodium or magnesium catalysts are slid on a small-scale and a large-scale test configuration to reveal the effect of softening or degradation on the sliding stability and to investigate possibilities for extrapolation of friction and wear rates between both testing scales. The combination of softening and afterwards transition into the glassy state is detrimental for the sliding stability of sodium catalysed polyamides, characterised by heavy noise during sliding. A transfer film formed under continuous softening also provides high friction. Melting during initial sliding is necessary for stabilisation in both friction and wear, and eventual softening of a molten film near the end of the test then not deteriorates the sliding stability. Softening of magnesium catalysed polyamides is favourable for the formation of a coherent transfer film resulting in more stable sliding than sodium catalysed polyamides. The differences in softening mechanisms of both polyamide grades is correlated to structural changes investigated by thermal analysis and Raman spectroscopy: the  $\gamma$  crystalline structure prevails in magnesium catalysed samples and the  $\alpha$  crystalline structure is predominant in sodium catalysed samples. For internal oil lubricated polyamides, a time dependent degradation of the polyamide bulk deteriorates the supply of internal oil lubricant to the sliding interface, resulting in high friction and wear under overload conditions. As the degradation mechanisms during sliding are strongly correlated to the test set-up, extrapolation is only possible for friction in a limited application range, while wear rates cannot be extrapolated.

© 2006 Elsevier Ltd. All rights reserved.

*Keywords:* Polyamide; Crystallisation; Raman spectroscopy

## 1. Introduction

Polymers are used for dry sliding applications as relatively soft materials with self-lubricating properties. The resistance against sliding is characterised by a horizontal friction force depending on normal load and sliding velocity. The friction and wear properties change, however, due to transfer of wear debris and formation of a polymer film on the steel counterface, often providing low friction and low wear rates.

Most of the mechanical energy consumed in the course of friction is transformed into heat, leading to a rise in temperature on the rubbing surfaces [1]. Degradation as softening, melting, oxidation and pyrolysis may therefore take place easily on the polymer surface and these processes further

control the sliding stability [2–5]. In some cases as, e.g. for ultra high molecular weight polyethylene (UHMWPE), softening under high loads is favourable for stable sliding [6]. Other polymers as, e.g. polyamides (PA) are, however, prone to overload and fracture [7]. Additives as oil or solid lubricants into the polyamide matrix improve the sliding stability, although it is not clear for those composites how the performance of fillers is affected by softening or melting of the bulk material.

The energy dissipation depends on the test-layout and as tribological testing is mostly done on a standardised pin-on-disc or bloc-on-ring tester, the performance under real working conditions may differ from the situation on laboratory scale. Also the sample area has a role in the energy dissipation and mainly for filled polymers, the supply of internal lubricant from the polymer bulk into the sliding surface is improved for large sliding areas. Besides applied normal loads and sliding velocities, degradation mechanisms are influenced by the testing scale. The practical application range of a sliding material is often characterised by a limiting

\* Corresponding author. Tel.: +32 3 264 33 08; fax: +32 9 264 32 95.

E-mail address: [pieter.samyn@ugent.be](mailto:pieter.samyn@ugent.be) (P. Samyn).

$p$  $v$  (pressure–velocity) value that is closely related to an acceptable wear rate at a certain temperature. In some cases, this limit can, however, be exceeded while the polymer still performs low friction and wear due to surface softening. Extremely high load conditions typically apply for design of bearing elements [8]. Extremely high sliding temperatures typically apply for processing of polymer melts [9]. The aim of this paper is:

- to reveal differences between degradation by softening and/or melting during sliding,
- to compare degradation mechanisms on both small-scale (low load/high velocity) and large-scale (high load/low velocity) sliding tests and analyse whether a small-scale test at high temperature can be extrapolated to large-scale tests at high load,
- to explore the polyamide performance under overload conditions,
- to explain differences in softening mechanisms and sliding stability by differences in polymer structure.

## 2. Experimental

### 2.1. Test materials

Three cast polyamide types are used as sliding material, i.e. pure polyamide that is sodium catalysed (PA–Na), pure nylon that is magnesium catalysed (PA–Mg) and polyamide PA–Na with a homogeneous dispersion of oil added during the casting process (PAo1). Mechanical parameters of the different grades are shown in Table 1 [10]. They are produced by Quadrant EPP by low pressure monomer casting, allowing for low process temperatures and polymerisation of molten lactam monomers right in the heated mould under atmospheric pressure. Characteristics of the polymerizing reaction during casting, such as initiation and propagation mechanisms, have been discovered with adding sodium as an activator, diisocyanates as a chain initiator and Na or Mg as a catalysor from liquid steams [11,12]. According to Kang et al. [13], the dispersion of oils becomes inhomogeneous in nylon for contents above 8 wt%. Test samples are machined from the bulk of cast elements, in order to avoid edge effects causing eventual inhomogeneities.

The counterfaces consist of cold rolled steel 42 CrMo4 (DIN 1.7225) with hardness 330 HV, yield strength  $R_e = 765 \text{ N/mm}^2$ , tensile strength  $R_m = 980\text{--}1180 \text{ N/mm}^2$  and chemical composition (wt%):  $C = 0.38\text{--}0.45$ ,  $Si < 0.40$ ,

$Mn = 0.60\text{--}0.90$ ,  $P < 0.035$ ,  $S < 0.030$ ,  $Cr = 0.90\text{--}1.20$ ,  $Mo = 0.15\text{--}0.30$ . Before each test, the surfaces were ground to an average surface roughness  $R_a = 0.20 \mu\text{m}$  measured parallel to the sliding direction and  $R_a = 0.60 \mu\text{m}$  perpendicular to the sliding direction. These values are representative for mainly an adhesive friction and wear type. Roughness is measured on a two-dimensional Perthen 5 SP according to DIN 4768. Prior to each test, polymer and steel surfaces were cleaned with acetone.

### 2.2. Sliding test equipment

Small-scale tests are done with a polymer cylinder (diameter 6 mm, length 12 mm) reciprocating sliding against a fixed steel counterface (58 mm  $\times$  38 mm). The polymer specimen is mounted by means of a clamp and center mechanism in a moving fixture, which provides an oscillating motion by a controlled variable speed motor through an eccentric power transmission for the adjustment of the stroke. A line contact is presently chosen for simulation of high contact pressures and easy alignment of the sliding pair. The steel counterface is connected to a base plate by means of four leaf springs with high stiffness in vertical direction and appropriate flexibility in horizontal direction. A normal load is manually applied through a spring and lever system that pulls down a bridge system over the polymer specimen. Contact between the bridge and the moving fixture is made by a roller bearing. A piezo-electrical force transducer with maximum capacity of 500 N in contact with the stationary steel plate is used to measure the horizontal reaction force that the polymer specimen exerts on the counterface. The counterface temperature can be controlled by means of resistance heating through four Vulstar cartridges.

A large-scale flat-on-flat tribotester is needed for investigating the effect of overload on large contact areas, related to the practical application of polyamides as bearing material possibly acting under yielding conditions. Two stationary polymer wear samples (150 mm  $\times$  150 mm) are mounted on top and bottom of a horizontally stiff frame and are in contact with the steel counterfaces (410 mm  $\times$  200 mm) that are positioned on top and bottom of a central sliding bloc. The latter moves reciprocating through the centre of the machine in contact with the polymer samples and is loaded by a vertical jack with maximum capacity of 6500 kN. Two dynamometers with maximum capacity of 2500 kN are in contact with the sliding bloc for recording the horizontal forces. The sliding velocity is controlled by a hydraulic circuit.

Table 1  
Mechanical properties of different polyamide grades (23 °C/60% RH)

| Test material | $d$ (g/cm <sup>3</sup> )   | $E$ (MPa) | $\sigma_y$ (MPa) | $\varepsilon$ (%) | Compressive stress (MPa) at nominal strain |    |    |    |
|---------------|----------------------------|-----------|------------------|-------------------|--|----|----|----|
|               |                            |           |                  |                   | 1%   | 2% | 5% |    |
| PA–Na         | Pure nylon Na catalysed    | 1.150     | 1700             | 55                | >50  | 26 | 51 | 92 |
| PA–Mg         | Pure nylon Mg catalysed    | 1.150     | 1500             | 75                | >50  | 23 | 42 | 82 |
| PAo1          | Homogeneous oil dispersion | 1.135     | 1450             | 45                | >50  | 22 | 43 | 79 |

The coefficient of friction  $\mu$  is determined by the ratio of horizontal forces and the applied normal load and wear rates are determined from weight measurements before and after testing. The latter values are compared to dimensional measurements of diameter reduction (small-scale) or thickness reduction (large-scale), allowing to estimate deformation by creep. Degradation of the polymer surfaces after sliding was examined by optical microscopy. Thermal analysis and Raman spectroscopy are used throughout the Section 4.

### 2.3. Test conditions

A broad range of normal loads and sliding velocities is used, as summarised in Table 2. First small-scale tests are done at 50, 100 and 150 N normal loads with a constant sliding velocity of 0.3 m/s. This corresponds to an initial Hertz contact pressure of 23, 33 and 41 MPa. The effect of an artificially implied temperature is verified by heating the steel counterfaces between 40 and 180 °C at 50 N, 0.3 mm/s. The latter overload conditions were applied in order to compare the behaviour at high temperatures and high loads whether they can compensate for each other. The total sliding distance is 6000 m with a single sliding stroke of  $s=15$  mm. Small-scale tests were repeated three times for each sliding parameter, showing typically  $\pm 7\%$  error on friction coefficients and  $\pm 10\%$  error on wear rates.

Large-scale tests are done at normal loads between 190 and 3440 kN, corresponding to 8–150 MPa, with a constant sliding velocity of 0.005 m/s and sliding stroke  $s=240$  mm. In case of no overload, the total sliding distance is 2000 m. Some overload tests were, however, stopped prematurely. The temperature rise only results from frictional heating as there is no possibility for external heating of the central sliding bloc. Large-scale tests were done two times with  $\pm 5\%$  error on friction coefficients and wear rates are averaged from four sliding blocs (each time positioned on top and bottom), showing  $\pm 7\%$  error.

### 2.4. Temperature calculation

In dry sliding, heat is conducted into both contact bodies through contact spots. Under high contact pressures, the real area of contact is close to the apparent area of contact and essentially a single contact occurs during sliding. For low contact stress situations, asperity interaction results in numerous temperature flashes [14] over areas of a few microns, causing local flow or melting. Because polymers are compliant, the local temperature rise is smaller than, for example, metal or ceramic contacts, where flash temperatures of 700 °C can occur. The real contact area enlarges through deformation of the polymer specimen, reducing the heat generated per unit of apparent area. Bulk temperatures can be experimentally measured over large contact areas, while different techniques to measure the transient temperatures at individual asperity contacts have been used with limited success [15].

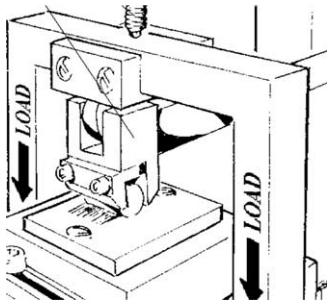
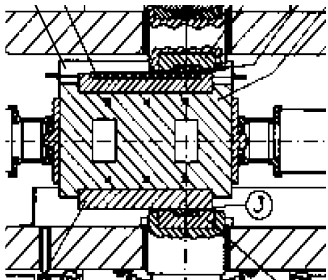
Two temperature models are presently evaluated for a rectangular moving heat-source ( $2\ell \times 2b$ , with  $\ell$  the semi-length in sliding direction,  $b$  the semi-width perpendicular to sliding direction). The length  $2\ell$  is found from the wear scar in case of small-scale tests or equals 150 mm in case of large-scale tests and the width  $2b$  equals 12 mm (small-scale) or 150 mm (large-scale). The generated frictional heat  $q = \mu p v$ , where  $p$  equals the contact pressure at regime and  $v$  the sliding velocity.

- According to Loewen and Shaw [16] the bulk temperature at the steel counterfaces is calculated from formula (1) for a stationary or low-velocity rectangular heat source

$$T_b = A \frac{\mu p v \ell}{k_1} \quad (1)$$

with  $A$  an area factor depending on the aspect ratio of the surface area ( $b/\ell$ ) and  $k_1 = 33$  W/mK. Bulk temperatures are experimentally verified with a K-type thermocouple placed on a given distance from the sliding stroke and corrected by a linear conductive law.

Table 2  
Test conditions for small-scale and large-scale sliding tests

| Testing scale    | Small-scale tribotester   | Large-scale tribotester  |
|------------------|---|--|
| Tribotester      |  |  |
| Normal load      | 50, 100, 150 N  | 190, 380, 560, 1260, 3440 kN   |
| Contact pressure | 23, 33, 41 MPa  | 8, 16, 25, 55, 150 MPa   |
| Sliding velocity | 0.3 m/s   | 0.005 m/s  |
| Sliding stroke   | 15 mm   | 240 mm   |
| Sliding distance | 6000 m  | 2000 m   |
| Temperature      | Free, 40, 80, 60, 100, 140, 180 °C  | Free   |

- A second temperature model according to Jaeger [17] is used for calculating flash temperatures at the polymer surface. Considering the formation of a polymer transfer layer with thermal conductivity  $k_2=0.29$  W/mK, and thermal diffusivity  $a=1.51 \times 10^{-7}$  m<sup>2</sup>/s, the general formulation (2) has been implemented towards Eq. (3). This model is developed for a moving heat source (strip or square) assuming that heat is dissipated through the contact asperities into a half space.

$$T_f = 1.13 \sqrt{\frac{\rho a \mu p v}{v k_2}} \quad (2)$$

$$T_f = 4.2 \times 10^{-4} \frac{\mu \sqrt{v} F_N}{\sqrt{\rho b}} \quad (3)$$

### 3. Test results

#### 3.1. Small-scale tests

##### 3.1.1. Influence of normal load

The coefficients of friction and flash temperatures as a function of the sliding distance are shown in Fig. 1 for PA–Na, PA–Mg and PAo1 at 50, 100 and 150 N. The corresponding wear rates are given in Table 3. Microscopic observations on

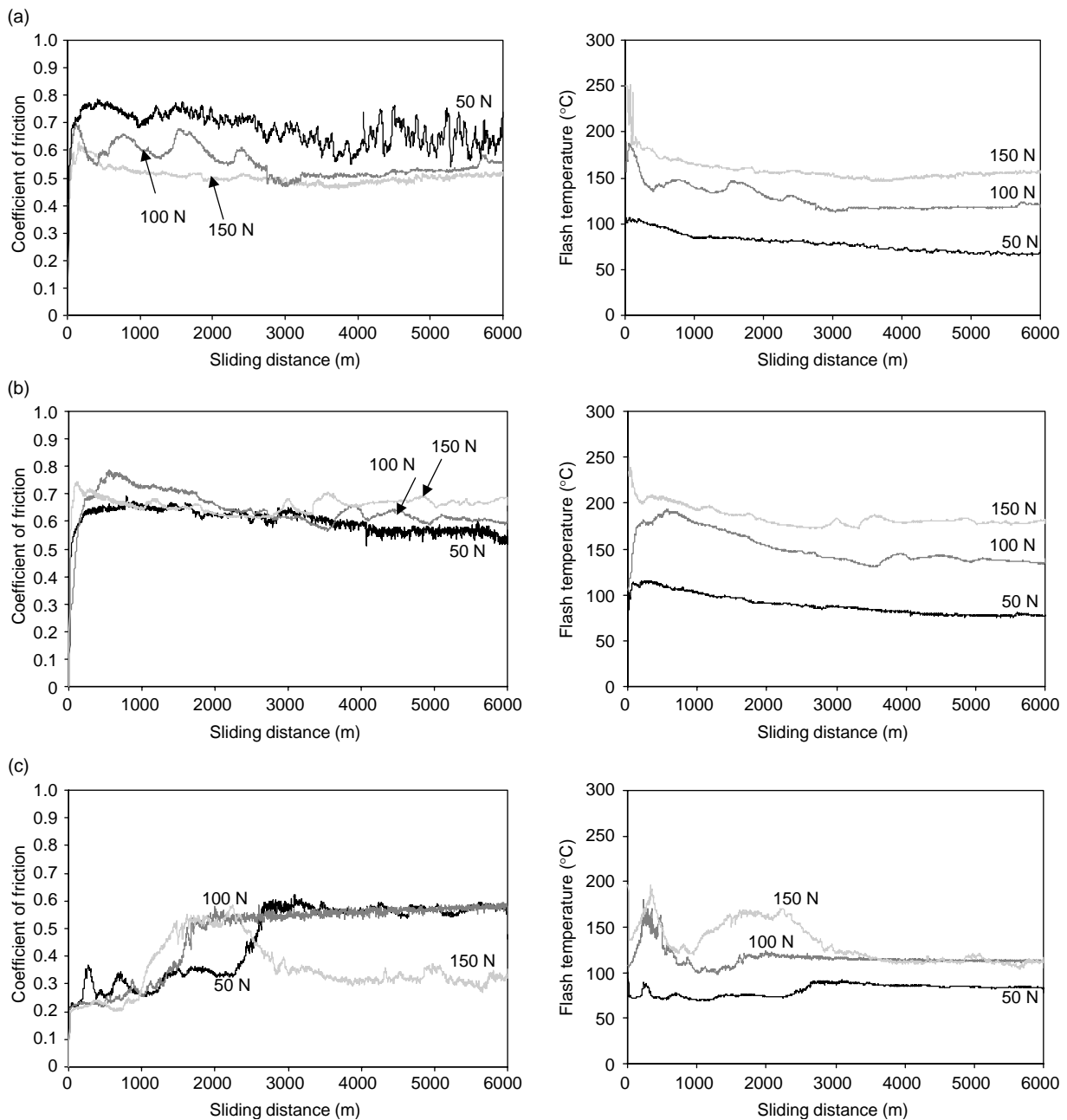


Fig. 1. Friction and flash temperatures for small-scale sliding at 50, 100 and 150 N for (a) PA–Na, (b) PA–Mg, (c) PAo1.

Table 3  
Small-scale weight loss ( $\Delta g$ ,  $10^{-4}$  g), diameter reduction ( $\Delta h$ , mm) and volumetric wear rates ( $w$ ,  $10^{-4}$  mm<sup>3</sup>/m)

|       | 50 N       |            |      | 100 N      |            |      | 150 N      |            |     |
|-------|------------|------------|------|------------|------------|------|------------|------------|-----|
|       | $\Delta g$ | $\Delta h$ | $w$  | $\Delta g$ | $\Delta h$ | $w$  | $\Delta g$ | $\Delta h$ | $w$ |
| PA–Na | 236        | 0.72       | 34.2 | 40         | 0.20       | 5.5  | 28         | 0.18       | 4.1 |
| PA–Mg | 78         | 0.27       | 11.3 | 46         | 0.25       | 6.8  | 39         | 0.23       | 5.6 |
| PAo1  | 64         | 0.25       | 9.4  | 260        | 0.70       | 38.2 | 58         | 0.30       | 8.5 |

the polymer surfaces and transfer to the steel counterfaces are illustrated in Fig. 2.

Friction and wear tendencies for pure PA–Na and PA–Mg are different at low and high loads (Fig. 1(a) and (b)). The 50 N test shows large fluctuations in friction of PA–Na and high wear rates originating from unstable sliding, while stabilisation in friction and lower wear rates occur at 150 N. The 100 N normal load is within a transition from unstable to stable sliding. Lower friction and smooth sliding was observed for PA–Mg compared to PA–Na at 50 N normal load, with consequently lower wear rates. At higher loads, this trend

reverses with higher friction and wear rates for PA–Mg than for PA–Na. These observations were the most important differences for sodium or magnesium catalysers. Oil-filled PAo1 (Fig. 1(c)) shows a transition into high friction after 2500 m sliding at 50 N, 1500 m sliding at 100 N and 1000 m sliding at 150 N. The high friction regime remains below the friction of pure PA–Na at 50 N, showing that the lubricating properties remain partially functional, while it becomes exactly similar to the friction of pure PA–Na at 100 N, showing that the lubricating activity completely fails. For the 150 N test, a second transition into low friction is observed after 2000 m

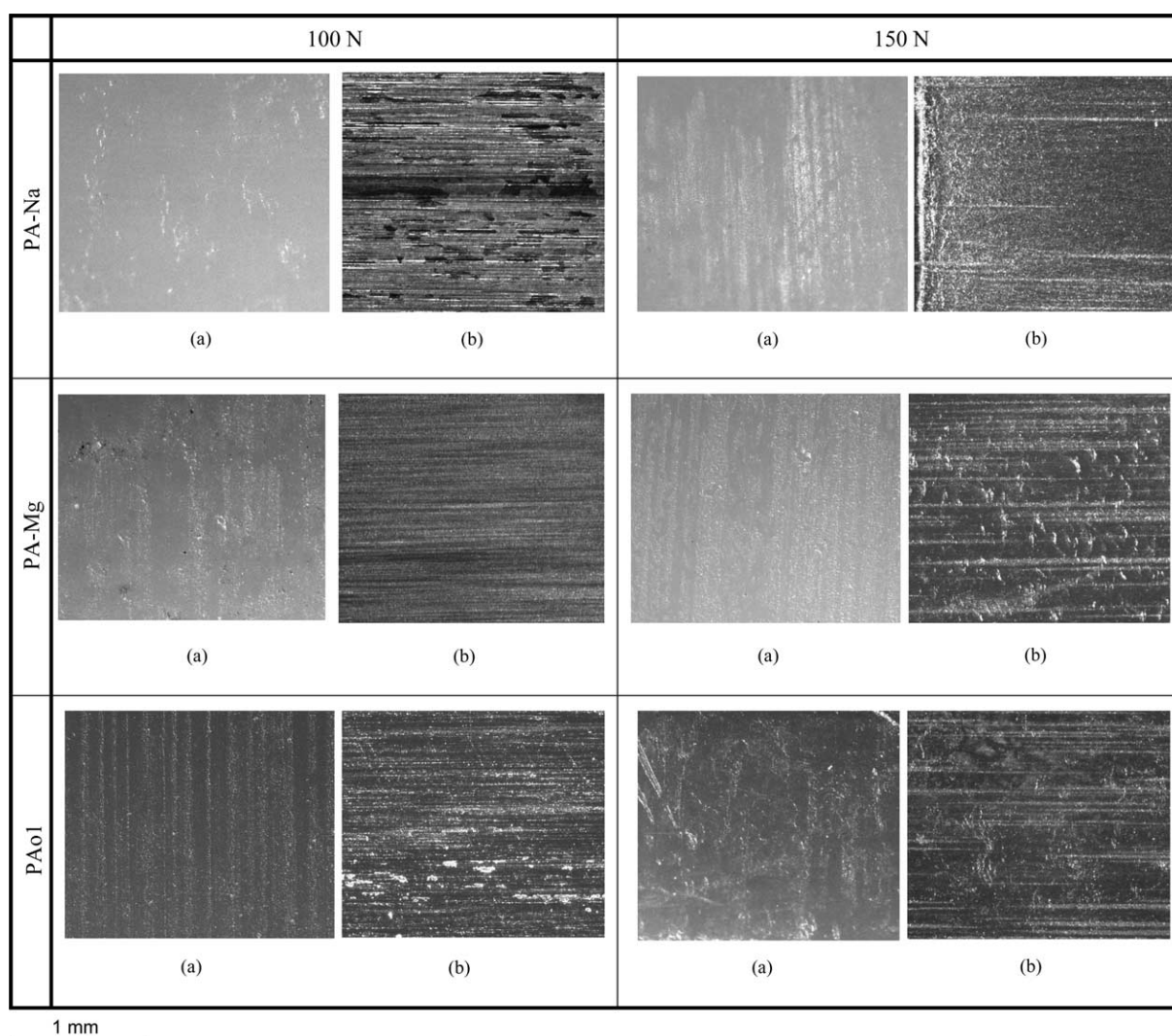


Fig. 2. Polyamide surfaces and transfer film after small-scale sliding, (a) polymer surface, (b) polymer transfer film on steel surface.

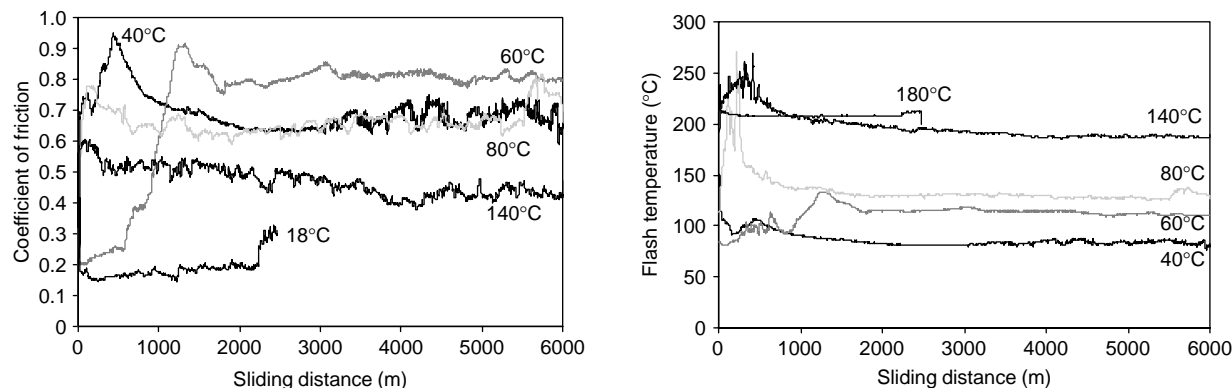


Fig. 3. Friction and flash temperatures for small-scale sliding of PA–Na at 50 N, with controlled bulk temperatures between 40 and 180 °C.

sliding. The wear rates of PAo1 are below those of pure polyamides only at 50 N while the high values at 100 and 150 N indicate overload, as the mechanical properties of oil-filled polyamide composites are lower than those of pure polyamides.

Related to the temperatures and surface aspect of PA–Na at 50 N, the flash temperature rises to 105 °C over only a short sliding time and decreases to 76 °C at the end of the test, below the glass transition temperature. It illustrates that softening of the polyamide surface is limited. A large amount of wear debris that was not compacted into a film is consequently observed and explains sliding instabilities. The flash temperature at 100 N rises to a maximum of 180 °C and attains 134 °C at the end of the test, indicating progressive softening with the formation of a coherent transfer film. It does, however, not completely stabilise the friction as the film is not molten and very brittle, while it is favourable for lowering wear rates. This mechanism is according to Lancaster [18] attributed to a decrease in counterface roughness. The flash temperature of 250 °C after short running-in at 150 N is favourable for melting and stabilisation of both friction and wear. As the flash temperature at the end of the sliding test is 173 °C, the initially molten film remains softened with good adhesion to the counterface.

The maximum and steady-state flash temperatures of 114 and 85 °C for PA–Mg at 50 N are higher than for PA–Na and the softening regime is maintained over the entire sliding test. Transfer is therefore even observed for a 50 N test. The flash temperature at 100 N attains 180–138 °C at 100 N and softening rather than melting mechanisms control the sliding of PA–Mg. A stable transfer film without brittle fracture forms. It is therefore concluded that softening mechanisms for PA–Na and PA–Mg are different and more favourable for stabilising friction in case of PA–Mg. Friction and wear is controlled by stable transfer film formation even at low load. Molten transfer for PA–Mg is observed at 150 N with flash temperatures above 200 °C. The film then becomes too weak and loses its load carrying capacity, resulting in higher wear rates.

The transition towards high friction for oil-lubricated PAo1 happens at a 90 °C flash temperature at 50 N or 110 °C at 100 N. The polymer surface only shows some abrasive wear

marks as characteristic softening mechanism. A decrease in friction at 150 N occurs for a 180 °C flash temperature. There is no exact correlation to a specific glass transition temperature of the polyamide bulk and a rather time–load related mechanism is supposed to interfere with the originally low friction. A remarkable change in transfer film is observed with lumpy polymer flakes at 50 and 100 N, while a homogeneous film with a large amount of oil develops at 150 N.

### 3.1.2. Influence of temperature

Pure PA–Na was also slid at 50 N on steel counterfaces heated between 40 and 180 °C (bulk temperatures), for implicitly simulating degradation effects of either softening or melting. The coefficients of friction and calculated flash temperatures are given in Fig. 3 and wear rates are presented in Table 4. Microscopy of the polyamide surfaces and transfer is illustrated in Fig. 4.

The coefficient of friction increases for 40–60 °C and decreases for 80–180 °C bulk temperatures. The wear rates gradually decrease between 40 and 100 °C in parallel to the effect of 50–150 N normal load. Friction and flash temperatures at 40 °C bulk temperatures are nearly similar to the 50 N test without temperature control (Fig. 1(a)) and like instabilities are observed at the end of the test. According to the calculated flash temperature for a 40 °C bulk temperature, the maximum temperature only attains 103 °C over a short sliding distance allowing for softening of the polymer surface, while it drops to 78 °C with consequent rubber into glassy transition. A thick and brittle transfer film develops as no melting happens, contributing to unstable sliding. Also for a 60 °C bulk

Table 4  
Small-scale weight loss ( $\Delta g$ ,  $10^{-4}$  g), diameter reduction ( $\Delta h$ , mm) and volumetric wear rates ( $w$ ,  $10^{-4}$  mm<sup>3</sup>/m) for tests at controlled bulk temperature with PA–Na

| Bulk temperature (°C) | $\Delta g$ | $\Delta h$ | $w$ |
|-----------------------|------------|------------|-----|
| 40                    | 20         | 0.09       | 2.9 |
| 60                    | 27         | 0.10       | 1.9 |
| 80                    | 12         | 0.08       | 1.7 |
| 100                   | 9          | 0.05       | 1.3 |
| 140                   | 55         | 0.17       | 8.2 |
| 180                   | 75         | 0.25       | 11  |

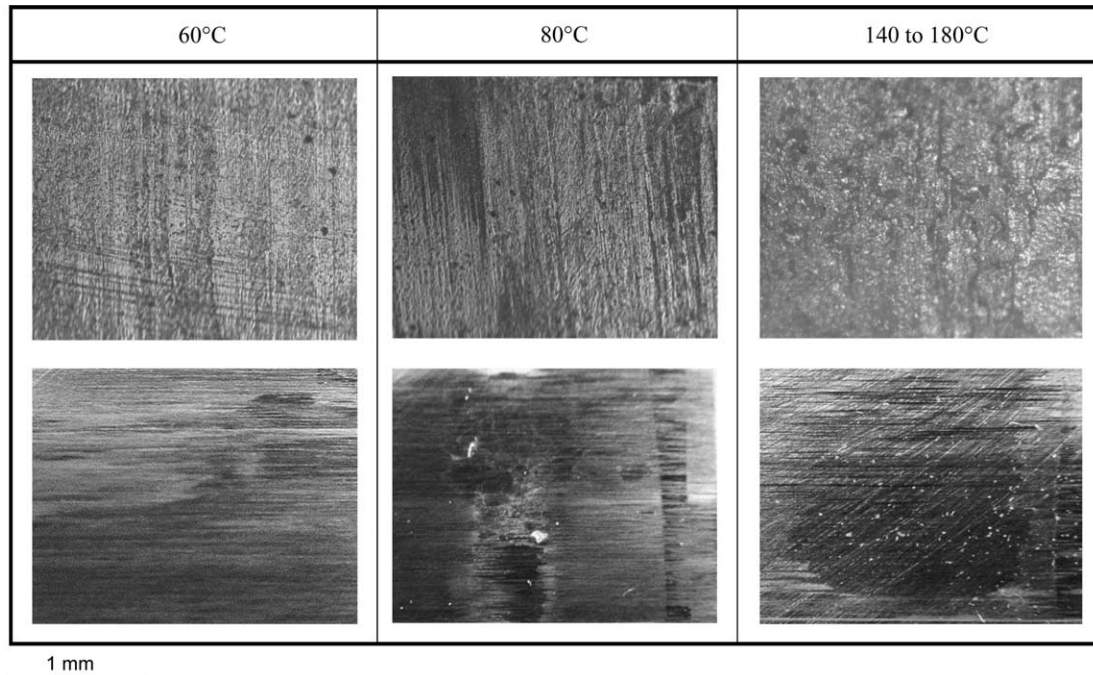


Fig. 4. Polyamide PA–Na surfaces (top) and transfer film (under) after small-scale sliding at controlled bulk temperatures of 60, 80 and 140–180 °C.

temperature, the flash temperature equals the softening temperature after 250 m of sliding with consequent formation of a thick transfer film, unstable sliding and increasing friction. The latter results in a further rise of flash temperatures to 135 °C, remaining below the melting temperature during the entire test run. Also in this case, the friction coefficient is unstable due to softening and its value is higher than at 40 °C bulk temperatures. The polymer surface only shows some grooves as slight deformation attributed to softening. For 80–140 °C bulk temperatures, the flash temperature during initial sliding attains the melting temperature of 220 °C and the surfaces remains softened till the end of the sliding test. The initial melting period seems favourable for lowering the coefficient of friction and mainly for the 140 °C bulk temperature test, continuous softening at 160 °C flash temperatures is favourable for progressively lowering the friction coefficient as a function of sliding time. This is reflected in a molten film on the steel surface with a thin molten layer in the centre and molten particles on the polyamide surface. But, however, bulk temperatures above 140 °C cause an increase in wear rates due to melting.

### 3.2. Large-scale tests

Fig. 5 presents friction coefficients and calculated bulk or flash temperatures for PA–Na, PA–Mg and PAo1 at 8–150 MPa as a function of logarithmic sliding distances, used for detailing the running-in process and the effect of a temperature rise above the glass transition temperature. Wear rates are given in Table 5. The polyamide surfaces are shown in Figs. 6–8. Experimental and calculated bulk temperatures under steady-state are evaluated in Table 6 and corrected with a value  $\Delta T = \mu p v s / k_1$  for a measuring depth  $s = 20$  mm.

According to formula (1), average bulk temperature  $T_{b,avg}$  is calculated from an area factor  $A = 0.95$  and maximum bulk temperature  $T_{b,max}$  from  $A = 1.12$  [16].

Friction for large-scale tests is generally lower compared to small-scale test conditions, while large-scale wear rates are higher. Extremely low friction is observed for a running-in period of approximately 10 m, but softening and melting mechanisms interfere with the transfer behaviour and result in higher and/or less stable friction. The latter transition is more clear than for small-scale tests. The initial period of low friction was not observed on small-scale tests (the first small-scale sliding cycles are detailed in Ref. [19] with friction 0.30–0.50).

For PA–Na at 8–16 MPa, the initial period of low friction in combination with low normal loads limits the flash temperatures to 46 and 72 °C. Similar to small-scale tests, friction at running-in is not favoured by softening and higher normal loads cause higher friction as plastification lacks. Once the flash temperature is above the glass transition, the sliding resistance increases due to a transition of the surface into the rubber phase. The maximum flash temperature of 166 °C at 8 MPa does not allow for melting and causes unstable sliding. At 16 MPa, only a short melting period enables slight surface melting and the formation of a transfer film that is beneficial for instantaneously decreasing the coefficient of friction. As the temperature, however, drops to 192 °C, re-solidification of the polymer surface and the transfer film also causes unstable sliding with fluctuations in friction and loud noise (stick-slip). Striations on the polyamide surface were also observed by Iwai et al. [20] during sliding of rubbers, indicating that the polymer surface is in a rubber-like phase and softening mechanisms prevail over melting at low loads. Immediate softening at 25–55 MPa decreases the running-in friction at

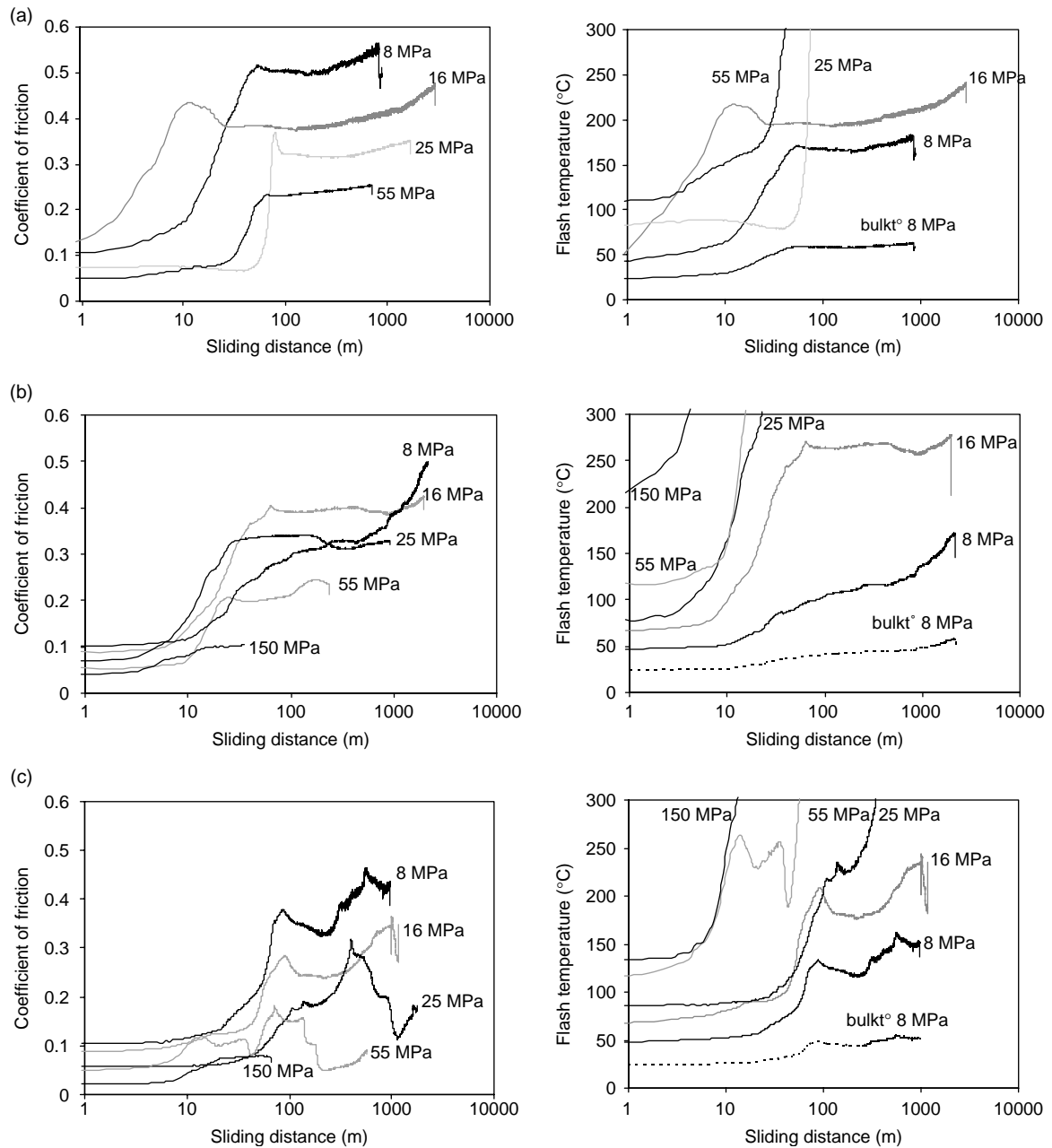


Fig. 5. Friction and sliding temperatures (dotted line represents bulk temperature at 8 MPa, other temperatures are flash temperatures) for large-scale sliding at 8, 16, 25, 55, 150 MPa for (a) PA–Na, (b) PA–Mg, (c) PAo1.

higher loads. Flash temperatures are above the melting temperature during steady-state with formation of a stable transfer film. The molten polyamide surface is characterised by irregular deformation. An increase in friction at 25 and 55 MPa for longer sliding times is not attributed to stick-slip

motion, but as the contact between polyamide and steel progressively converts into a polymer/polymer contact, the adhesive component of friction increases. Adhesive forces for polyamides are important due to high surface energy (polarity) [21].

Table 5

Large-scale volumetric wear rates weight loss ( $w_g$ ,  $\text{mm}^3/\text{m}$ ) and thickness reduction ( $w_t$ ,  $\text{mm}^3/\text{m}$ ) with indication of the percentage creep deformation (%)

|       | 8 MPa |       |    | 16 MPa |       |    | 25 MPa |       |    | 55 MPa |       |    |
|-------|-------|-------|----|--------|-------|----|--------|-------|----|--------|-------|----|
|       | $w_g$ | $w_t$ | %  | $w_g$  | $w_t$ | %  | $w_g$  | $w_t$ | %  | $w_g$  | $w_t$ | %  |
| PA–Na | 1.4   | 1.9   | 26 | 9.0    | 10.9  | 17 | 9.1    | 11.4  | 20 | 51     | 63    | 20 |
| PA–Mg | 0.8   | 0.9   | 11 | 12.0   | 14.2  | 15 | 69.7   | 88.0  | 21 | 198    | 256   | 25 |
| PAo1  | 1.1   | 1.6   | 31 | 1.7    | 2.2   | 22 | 4.9    | 6.8   | 27 | 38     | 61.7  | 38 |



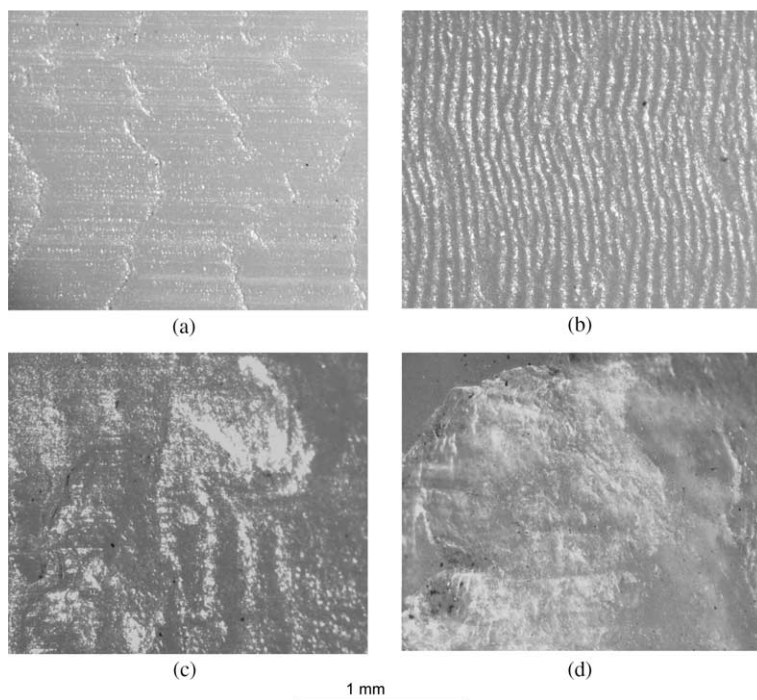


Fig. 6. Polyamide PA–Na surfaces after large-scale sliding at different normal loads, (a) 8 MPa, (b) 16 MPa, (c) 25 MPa, (d) 55 MPa.

The running-in performance for PA–Mg at 8 MPa is identical to PA–Na with a friction coefficient 0.1 and 46 °C flash temperature. A different trend, however, develops at steady-state, as the friction for PA–Mg progressively increases while remaining below PA–Na. The flash temperature attains the glass transition temperature after 25 m of sliding and it does

not dramatically increase the friction or it does not cause unstable sliding as observed for PA–Na. On the contrary, softening seems favourable for slowing down the increase in friction: within the softening regime (23–30 m sliding) there is a slight increase in friction, attributed to lowering the mechanical strength and enhanced ploughing component of

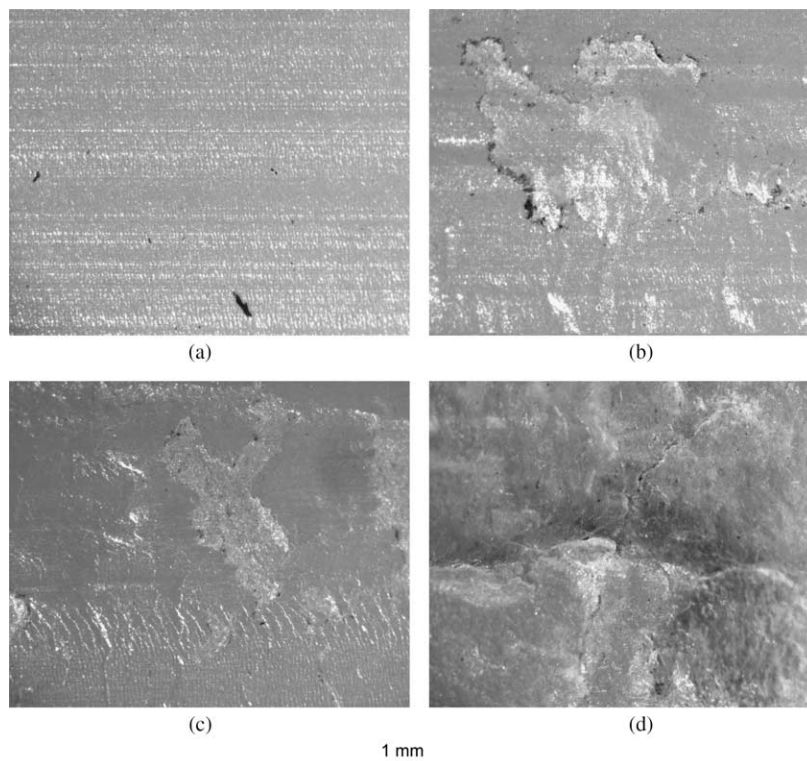


Fig. 7. Polyamide PA–Mg surfaces after large-scale sliding at different normal loads, (a) 8 MPa, (b) 16 MPa, (c) 25 MPa, (d) 55 MPa.

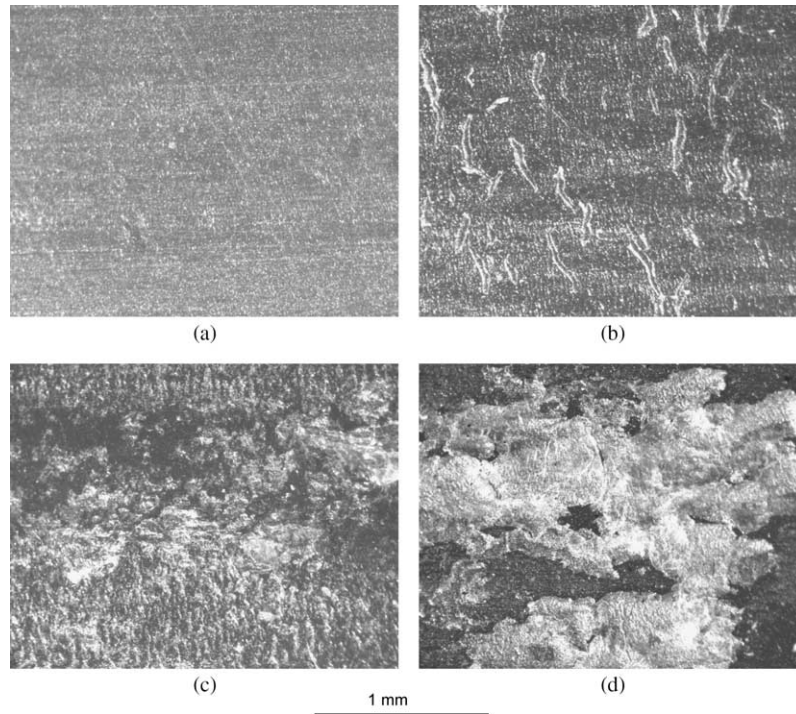


Fig. 8. Polyamide PAo1 surfaces after large-scale sliding at different normal loads, (a) 8 MPa, (b) 16 MPa, (c) 25 MPa, (d) 55 MPa.

friction, but the friction slope between 30 and 900 m sliding lowers as a coherent transfer layer forms. The melting temperature is not attained and adhesion effects between polymer/polymer contacts mentioned above explain the rise in friction after 900 m sliding at 8 MPa. The differences in friction between PA–Mg and PA–Na as observed on small-scale tests under low loads are thus also reflected in large-scale testing. From 16 MPa on, the running-in friction monotonously decreases at higher load, in contrast to the situation of PA–Na and independently of the initial flash temperature being below or above the glass transition temperature. Due to high contact pressures between 16 and 55 MPa, melting of PA–Mg during steady-state sliding results in polymer transfer and friction behaviour nearly similar to PA–Na, controlled by adhesion. The wear rates have a similar trend to the frictional behaviour: lower wear for PA–Mg at 8 MPa and large wear at 16–55 MPa compared to PA–Na. This is in accordance to small-scale tests of PA–Mg and PA–Na.

For PAo1 at running-in, the friction for a 8–16 MPa test is some higher than for 25–150 MPa as the glass transition temperature is exceeded in the latter cases. Similar to PA–Na, friction for PAo1 at 8 and 16 MPa does not stabilise under steady-state with a nearly identical temperature profile for both materials. Unstable sliding for PAo1 is explained by the formation of a softened transfer layer with insufficient melting, as called ‘lumpy transfer’. The lack of melting is also reflected in the reasonable low wear rates 1–1.7 mm<sup>3</sup>/m. Similar tendencies were observed on small-scale tests at 50 or 100 N. For large-scale testing at 25–55 MPa, the running-in behaviour controlled by softening is identical as for pure PA–Na, although melting at either 100 or 10 m sliding causes large fluctuations in friction through a combination of lubricant supply, deformation, transfer film build-up and removal. Attributed to melting mechanisms at 25 and 55 MPa, it shows high wear rates with final overload at 150 MPa.

Table 6  
Correlation between experimental and calculated bulk temperatures for PA–Na and PA–Mg

|       | P (MPa) | Calculated temperatures $\theta$ (°C) from measured bulk temperatures T (°C) |            |                            |             | Temperature analysis by Loewen and Shaw |  |
|-------|---------|--|------------|----------------------------|-------------|---|--|
|       |         | Measured bulk temperature  | $\Delta T$ | Corrected bulk temperature | $T_{b,avg}$ | $T_{b,max}$                             |  |
| PA–Na | 8       | 38   | 13         | 51                         | 46          | 54                                      |  |
|       | 16      | 58   | 21         | 79                         | 74          | 87                                      |  |
|       | 25      | 63   | 25         | 88                         | 86          | 100                                     |  |
|       | 55      | 92   | 38         | 130                        | 136         | 160                                     |  |
| PA–Mg | 8       | 39   | 12         | 51                         | 44          | 52                                      |  |
|       | 16      | 50   | 20         | 70                         | 71          | 84                                      |  |
|       | 25      | 57   | 24         | 81                         | 86          | 101                                     |  |
|       | 55      | 80   | 35         | 115                        | 124         | 146                                     |  |

## 4. Discussion

### 4.1. Thermal analysis, structural properties and tribological performance of unfilled cast polyamides

It was demonstrated on both small-scale and large-scale tests that the coefficient of friction is strongly influenced by softening and/or melting of polyamides. The combination of softening and transition into the glassy state is detrimental for the sliding stability of PA–Na, characterised by heavy noise. A transfer film formed by continuous softening also provides high friction. Melting during initial sliding is necessary for stabilisation in both friction and wear, and eventual softening of a molten film near the end of the test then not deteriorates the sliding stability. Softening of PA–Mg at low loads seems favourable for the formation of a coherent transfer film and more stable sliding than PA–Na.

Differences in softening characteristics are related to the polymer structure by thermal analysis of the unworn polymer (Fig. 9) and FT-Raman scattering of both unworn (Fig. 10(a)) and worn (Fig. 10(b)) surfaces:

- Simultaneous thermogravimetric analysis (TGA) and differential thermal analysis (DTA) was done on a Stanton Redcroft Thermobalance STA 1500 under inert nitrogen atmosphere. Measurements were standardised by running a thermograph on an empty  $\text{Al}_2\text{O}_3$  crucible. Polyamide samples of 12 mg were heated in one single step from 23 to 300 °C at 10 °C/min. For TGA a sensitive balance is used to follow the weight change of the sample as a function of temperature. In DTA the polyamide sample and an inert  $\text{Al}_2\text{O}_3$  reference sample, undergoing no thermal transition in the temperature range to 300 °C, were heated at the same rate while the temperature difference was plotted as a function of the sample temperature (Fig. 9), showing the endotherm melting temperature. Each polyamide grade shows decreasing weight above its glass transition temperature to a final loss of 3% for PA–Na, 4% for PAo1 and 6% for PA–Mg. The degradation of PA–Mg is more significant than for PA–Na, mainly in the

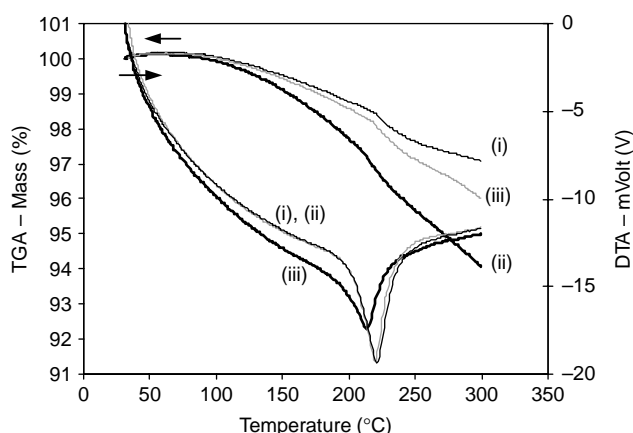


Fig. 9. Characterisation of different polyamide grades by thermal analysis (DTA–TGA), (i) PA–Na, (ii) PA–Mg, (iii) PAo1.

softening region 90–220 °C. Softening starts at 88 °C for PA–Mg and at 95 °C for both PA–Na and PAo1. The melting temperature is 220 °C for PA–Na and PAo1, while it is 215 °C for PA–Mg. The latter shows a broad peak with onset at 187 °C. A narrow melting peak with onset at 195 °C coincides for PA–Na and PAo1 and good agreement in thermal behaviour is found as PA–Na is used as bulk material for the oil-filled polyamide composite. However, the somewhat higher weight loss of PAo1 compared to PA–Na is attributed to thermally activated oil discharge, starting in the 60–80 °C temperature range according to Yabe et al. [22]. For a 70 wt% oil-impregnated material, they found 2 wt% immediate discharge rate and 8–10 wt% discharge rate after 10,000 h. Marchetti et al. [23] found 3–4 wt% loss in polyimides during migration experiments of oil under static conditions during 4 days at 60 °C. As polyimides have high thermal stability, no interference between lubricant supply and softening or melting happened.

- FT-Raman spectroscopy gives additional information of the polyamide structure, not only on the chemical composition but also on crystallinity. Measurements were done on a Bruker FT spectrometer Equinox 55S (Bruker Optik, Ettlingen, Germany), equipped with a Raman module FRA 106 fitted to a nitrogen cooled (77 K) germanium high sensitivity detector D418-T. The polymer samples were excited by a 1064 nm beam from a Diode Laser Pumped Nd:YAG laser. The laser power was adjusted at 150 mW with a probe area of 1 mm<sup>2</sup>. The scattered light was collected at an angle of 0° and the spectral resolution is 3 cm<sup>-1</sup>. The spectra as in Fig. 10 were obtained from multiple scanning and averaged over 250 measurements at 10 locations over the surface. Data collection and data transfer was automated using the Bruker OPUS™ software.

The frequency range of interest in the spectra of PA–Na, PA–Mg and PAo1 is at 900–1000 and 1000–1700 cm<sup>-1</sup>. Unworn samples (Fig. 10(a)) show good correspondence in the spectra for PA–Na and PAo1 and good reproducibility of the Raman measurements. The amide I (C=O) band at 1636 cm<sup>-1</sup> is identical for each polyamide grade while the amide III (N–H bending and C–N stretching vibrations) band at 1280 cm<sup>-1</sup> has a lower intensity for PA–Mg. Variations in some bands of PA–Mg and PA–Na are noticed, most prominently at the 962 and 1079 cm<sup>-1</sup>. The spectra are analysed according to Ferreiro et al. [24] or Schmidt et al. [25], assigning Raman wavenumbers to a specific polyamide structure.

Three crystalline structures of PA 6 are widely described in literature [26,27], i.e. the monoclinic  $\alpha$ , the pseudo-hexagonal  $\beta$  and the monoclinic  $\gamma$ . The  $\alpha$  and  $\gamma$  crystalline structures have been well characterised by X-rays and FTIR analysis [28]. Based on reference Raman spectra for each structural composition, the band at 1127 cm<sup>-1</sup> characterises a planar band representative for fully extended chains with the amide groups in the same plane as the methylene groups, only present in the  $\alpha$  crystalline form according to Holmes et al. [29].

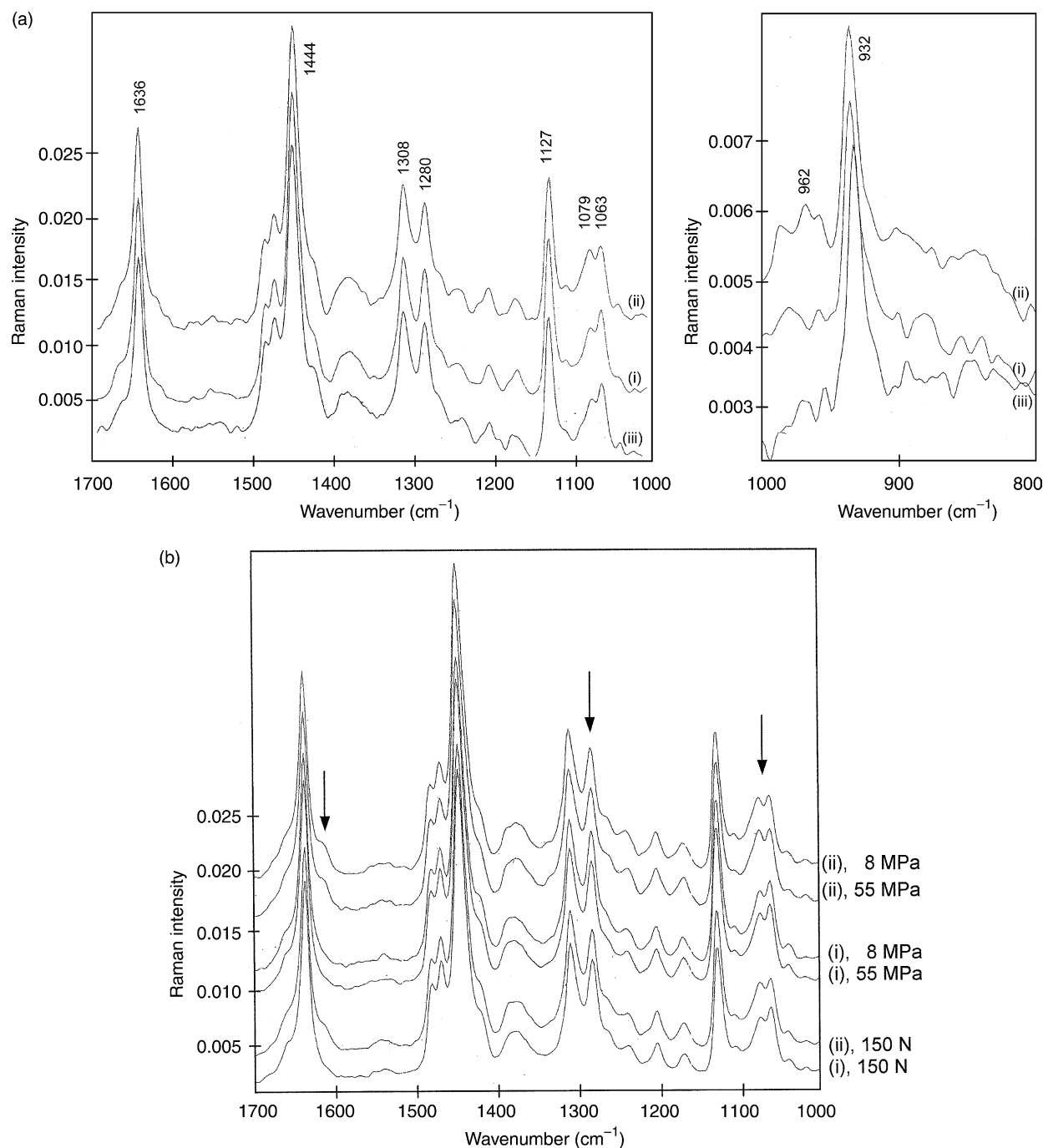


Fig. 10. Raman spectra of different polyamide grades, (a) unworn, (b) worn at 8 and 55 MPa large-scale and 150 N small-scale, (i) PA–Na, (ii) PA–Mg, (iii) PAo1.

The band at  $1079\text{ cm}^{-1}$  is characteristic for a twisted or non-planar configuration: Arimoto et al. [30] showed that the amide group in the  $\gamma$  structure is rotated  $67^\circ$  away from the main chain. Hydrogen bonds occur between parallel chains and the interchain distance for the  $\gamma$  form is higher than for the  $\alpha$  form [31]. The  $\beta$  structure is a mesomorphous phase that is obtained upon quenching the molten polymer.

Although the cast samples are a mixture of different crystalline phases, some bands indicate that the  $\gamma$  structure prevails in the PA–Mg samples and the  $\alpha$  structure is predominant in the PA–Na samples. The clearest evidence is

found in the intensity ratio of the bands  $I_{1079}/I_{1127}$  being higher for PA–Mg than for PA–Na or PAo1. Also the less prominent  $1063\text{ cm}^{-1}$  band in PA–Mg suggests a  $\gamma$  structure. The lower intensity  $I_{1127}/I_{1444}$  with a nearly constant ratio  $I_{1444}/I_{1636}$  for PA–Mg relatively to PA–Na confirms this trend. In case of PA–Na, the intensity  $I_{1079}/I_{1127}=0.42$  is in good correspondence with a reference spectrum of pure  $\gamma$  polyamide. From a reference spectrum of pure  $\gamma$  polyamide, the estimated content  $\gamma$  polyamide in PA–Mg is 15–20%. Minor indications of a prevailing  $\gamma$  structure for PA–Mg are observed in accordance with Jakes et al. [32] and Vansanhan et al. [33]. The existence

of a supplementary band at  $962\text{ cm}^{-1}$  and a shoulder band at  $1234\text{ cm}^{-1}$  for PA–Mg was also observed for PA 6  $\gamma$  films by Ferreiro et al. [24]. From an overview in the latter work, some bands shift significantly to a lower wavenumber in the  $\gamma$  structure relatively to the  $\alpha$  structure. This is presently also observed—although not as strongly as revealed on pure  $\alpha$  or  $\gamma$  structures—, e.g. from  $1127.79\text{ cm}^{-1}$  for PA–Na to  $1127.54\text{ cm}^{-1}$  for PA–Mg, as attributed to the different positions of the C–C amorphous stretch.

Penel-Peirron et al. [34] prepared pure  $\alpha$  and  $\gamma$  structured PA 6 samples and performing DSC measurements, a melting peak of  $220\text{ }^\circ\text{C}$  for  $\alpha$  crystals and  $215\text{ }^\circ\text{C}$  for  $\gamma$  crystals was noted. The lower melting point of PA–Mg presently revealed from TGA-DTA then agrees with Raman measurements indicating a prevailing  $\gamma$  structure of the PA–Mg samples and  $\alpha$  structure in PA–Na. The  $\gamma$  phase is thermally stable up to  $200\text{ }^\circ\text{C}$  without transition into another crystalline form [35], corresponding to the onset of the melting peak of PA–Mg. According to patent literature [36], it is very likely that different catalytic processes induce a different crystalline structure as also mentioned in publications of Penel-Peirron et al. [34–35] using a nucleating agent to prepare intentionally  $\gamma$  structured polyamides. Other possibilities for  $\gamma$  crystallisation are lower processing time and crystallisation temperatures. Rapid cooling after casting and a low crystallisation temperature generally promote the  $\gamma$  form of PA 6, while higher crystallisation temperatures or a slow cooling rate lead to the  $\alpha$  form [37].

As PA–Mg has different sliding behaviour compared to PA–Na, also differences in plasticity were noticed under tensile testing [38]. Polyamide samples in the mesomorphic  $\beta$  form are more ductile than in the predominant  $\alpha$  form, while the  $\gamma$  crystalline form has lower yield stress and higher ductility compared to the brittle  $\alpha$  crystals. Also Bessell et al. [39] and Bell et al. [40] showed that decreasing crystallinity improves the PA 6 ductility. Comparing the damping factor  $\tan \delta$  for  $\alpha$  and  $\gamma$  phase polyamides [34] shows slightly higher chain mobility for the  $\gamma$  polyamide in the temperature range  $40\text{--}80\text{ }^\circ\text{C}$ . Also Ito et al. [41] reported that polyamide films coextruded in the solid state in the temperature range  $100\text{--}180\text{ }^\circ\text{C}$  have better ductility in the  $\gamma$  form than in the  $\alpha$

form. As PA 6 plasticity is basically governed by crystal slip parallel to the hydrogen bonded sheet structure, i.e. without rupture of the H bonds [42], the lower H-bond density in the  $\gamma$  form could not explain plastic deformation. It seems mainly influenced by the higher intersheet distance of the  $\gamma$  crystals and consequently lower critical shear stresses. As observed by AFM [24], plastic deformation occurs through nucleation and propagation of the shear bands in the amorphous phase. The ductility of PA–Mg attributed to a prevailing  $\gamma$  phase compared to PA–Na is presently also reflected in the sliding tests by lower wear rates at  $50\text{ N}$  on small-scale or at  $8\text{ MPa}$  on large-scale sliding tests for PA–Mg compared to PA–Na.

Strain induced  $\gamma$  to  $\alpha$  transitions above  $120\text{ }^\circ\text{C}$  has been studied during tensile testing [35], however, it is not clear whether this process is stress and/or thermal activated. According to Miyasaka et al. [44] the  $\gamma$  phase is mechanically reasonably stable and its transformation into  $\alpha$  is limited, not providing higher mechanical strength. Possible  $\gamma$  to  $\alpha$  transitions after small-scale and large-scale sliding tests are presently studied from the spectra of worn PA–Na and PA–Mg samples in Fig. 10(b). The  $I_{1079}/I_{1127}$  and  $I_{1063}/I_{1127}$  relative intensities before and after sliding are given in Table 7. A slight conversion of  $\gamma$  into  $\alpha$  structure after sliding of PA–Mg can be noted from following observations: (i) the  $\gamma$ -related intensity  $I_{1079}/I_{1127}$  decreases from 0.50 to 0.48 (large-scale) or 0.46 (small-scale), slightly evolving to the values of PA–Na that have an  $\alpha$  structure and low  $I_{1079}/I_{1127}$  values, and (ii) the  $1127.54\text{ cm}^{-1}$  band for PA–Mg slightly shifts upward to  $1128\text{ cm}^{-1}$  after large-scale sliding or towards  $1128.18\text{ cm}^{-1}$  after small-scale sliding. This indicates that the  $\gamma$  into  $\alpha$  transition for PA–Mg is most pronounced for small-scale tests, favoured by high sliding velocities and better orientation. The intensities for PA–Na are lower and less affected by sliding, as it has an overall  $\alpha$  structure that is more stable.

Variations in the amide I band ( $1636\text{ cm}^{-1}$ ) resulting from the C=O stretching vibration after sliding, relatively to the amide III band ( $1280\text{ cm}^{-1}$ ), are different after either large-scale or small-scale testing. Reorientation after small-scale testing occurs nearly to the same extent for each sliding parameter, while it develops more progressively during

Table 7  
Relative intensities of some Raman bands before and after sliding

| Test conditions                   | Crystalline structures |       |                     |       | Amide I/Amide III   |       |
|-----------------------------------|------------------------|-------|---------------------|-------|---------------------|-------|
|                                   | $I_{1079}/I_{1127}$    |       | $I_{1063}/I_{1127}$ |       | $I_{1636}/I_{1280}$ |       |
|                                   | PA–Na                  | PA–Mg | PA–Na               | PA–Mg | PA–Na               | PA–Mg |
| Unworn                            | 0.42                   | 0.50  | 0.54                | 0.53  | 1.61                | 1.71  |
| Small-scale test                  |                        |       |                     |       |                     |       |
| 50 N                              | 0.44                   | 0.48  | 0.51                | 0.52  | 1.73                | 1.73  |
| 100 N                             | 0.40                   | 0.46  | 0.51                | 0.50  | 1.72                | 1.70  |
| 150 N                             | 0.40                   | 0.46  | 0.50                | 0.50  | 1.73                | 1.73  |
| 50 N, $140\text{ }^\circ\text{C}$ | 0.40                   | 0.45  | 0.48                | 0.50  | 1.74                | 1.74  |
| Large-scale test                  |                        |       |                     |       |                     |       |
| 8 MPa                             | 0.42                   | 0.50  | 0.48                | 0.51  | 1.67                | 1.70  |
| 25 MPa                            | 0.42                   | 0.48  | 0.47                | 0.50  | 1.72                | 1.72  |
| 55 MPa                            | 0.42                   | 0.48  | 0.47                | 0.48  | 1.77                | 1.74  |

large-scale testing. Also a shoulder band at the amide I band disappears after sliding PA–Na while it remains existing after sliding PA–Mg; Raman spectra studied by Stuart [43] at high temperatures indicated an increase in C=O stretching frequency as the effect of loosening intermolecular hydrogen-bonding and crystallisation.

#### 4.2. Effectiveness of internal lubrication mechanisms

Sliding instabilities for oil-filled PAo1 are related to interactions between oil supply mechanisms and softening. Means of supplying lubricant to the interface were studied by Marchetti et al. [22] and are attributed to ‘static’ effects through free spaces or pores in the matrix (migration, capillary effects caused by the surface roughness and Maragoni effects due to temperature gradients) and ‘dynamic’ effects (centrifugation).

The low flash temperatures of 77 °C during small-scale sliding at 50 N do not promote thermal migration. As oil at the surface becomes exhausted during sliding, there is a sudden increase in friction and wear, promoting fresh lubricant exhibited at the surface and lowering of friction. These recurrent processes repeat until the flash temperature attains the glass transition temperature and blocks the migration paths by deformation. The sliding situation is then comparable to pure PA–Na. At 100–150 N, the running-in wear of PAo1 is significantly lower and suggests that previous recurrent processes are less likely, while thermal migration effects during running-in become more evident. Immediate softening at flash temperatures above 120 °C and shortly at 180 °C allows for combined transfer of polyamide and oil with low running-in friction at 100 N, although the solidification during cooling to 117 °C restricts further lubrication. It is visually noted that the transfer film then contains separate polyamide flakes and only a limited amount of oil. The 180 °C flash temperature is maintained for a long sliding time at 150 N and causes a large exposure of liquid oil as revealed on the transfer film and transition towards low friction and stable wear. The transitions in lubrication mechanisms for 100–150 N are, however, less correlated to a softening or melting temperature of the polyamide bulk, showing that the processes rather relate to loading time and shear deformation. Transitions for large-scale tests are also not closely related to a specific transition temperature, while it is rather a time-load related phenomenon that also depends on the sample area.

#### 4.3. Extrapolation

For extrapolation of friction and wear between small-scale and large-scale configurations, Czichos [45] provided a scheme where an equal amount of mechanical and hermal input is assumed. Scaling resulted sometimes in premature failure [46]. Mainly for polymers, thermal transitions in structure and differences in transfer film formation may alter the tribological performance. It is also clear from previous discussion that scaling of test results for internal lubricated polymers is difficult to make due to degradation of the lubricant mechanism.

Scaling effects were evaluated in previous work on polyacetals [47] by introducing a geometrical factor  $G$  and the Peclet number  $Pe$ . The parameter  $p\nu\sqrt{PeG}$  ( $W/m^2$ ) chosen as scaling parameter correlates to contact temperature, with:

- $Pe = v\ell/k$ , which is constant for large-scale sliding ( $Pe = 64$ ) and variable for small-scale sliding ( $26 < Pe < 51$ ). Under both conditions  $Pe > 10$ , ranging in the high-speed category.
- $G =$  macroscopic geometry parameter  $= 2\ell b/s(\ell + b)$ , depending on the ratio of contact area to contact contour and the sliding stroke  $s$ .

The friction coefficients from both small-scale and large-scale tests are plotted in Fig. 11 for PA–Na and PA–Mg together with the regime sliding temperature as a function of the scaling factor. The temperatures increase linearly and match for both large-scale and small-scale sliding tests, changing in slope above the melting point.

Friction for PA–Na shows a fitting trend on both small-scale and large-scale tests, allowing for extrapolation. The coefficient of friction decreases for small-scale tests in the flash temperature range between 50 and 150 °C and it further decreases on large-scale tests with flash temperatures above 220 °C. A friction coefficient of 0.5 remains, however, constant in the temperature region between 150 and 180 °C. Different trends are, however, noted for PA–Mg: the coefficient of friction increases both on large-scale and small-scale tests for temperatures below the melting point, while it decreases for higher temperatures, allowing for extrapolation only in this region. The small-scale sliding tests on PA–Na at controlled bulk temperatures are not able to compensate for the high loads on large-scale tests.

The relation of friction with normal load and sliding velocity is described by literature models for small-scale tests [48]. For polymers, the general law of friction  $F_{\text{friction}} = \mu F_N$  with constant  $\mu$  as a function of  $F_N$  is not true due to visco-elastic deformation. Therefore, the friction coefficients follow the equation  $\mu = KF_N^{(n-1)}$ , where  $K$  and  $n$  are constants with  $2/3 < n < 1$ , depending on the interaction between elastic and plastic deformation. Models for thermally controlled friction indicate a reduction in friction, according to  $\mu = KF_N^{0.25}$  for partial contact to  $\mu = KF_N^{(n-1)}$  for full contact. From sphere-on-flat tests, a basic relation between the coefficient of friction and normal load was developed by Pascoe and Tabor for nylon 66 [49] in a load range of  $10^{-4}$ – $10^4$  g, corresponding to  $p_{\text{max}} = 207$  MPa and  $p_{\text{mean}} = 138$  MPa for under  $10^4$  g. They mentioned that the experimental slope of  $\mu$  against  $F_N$  at high loads is less steep than the theoretical curve. Present small-scale and large-scale experiments fit to a power law  $p^{-0.24}$  for PA–Na or  $p^{-0.36}$  for PA–Mg with, however,  $R^2 < 0.9$  indicating low correspondence. According to the scaling parameter presently defined, the fitted trend line on PA–Na with an exponent  $-1/3$  ( $R^2 = 0.97$ ) is in better agreement with a general power law of Yamaguchi [50], assuming the coefficient of friction  $\mu$  proportional to  $p^{-1/3}$ . An exponent  $-2/3$  ( $R^2 = 0.99$ ) from the trend line on PA–Mg indicates higher influence of the softening and crystallisation mechanisms as described above.

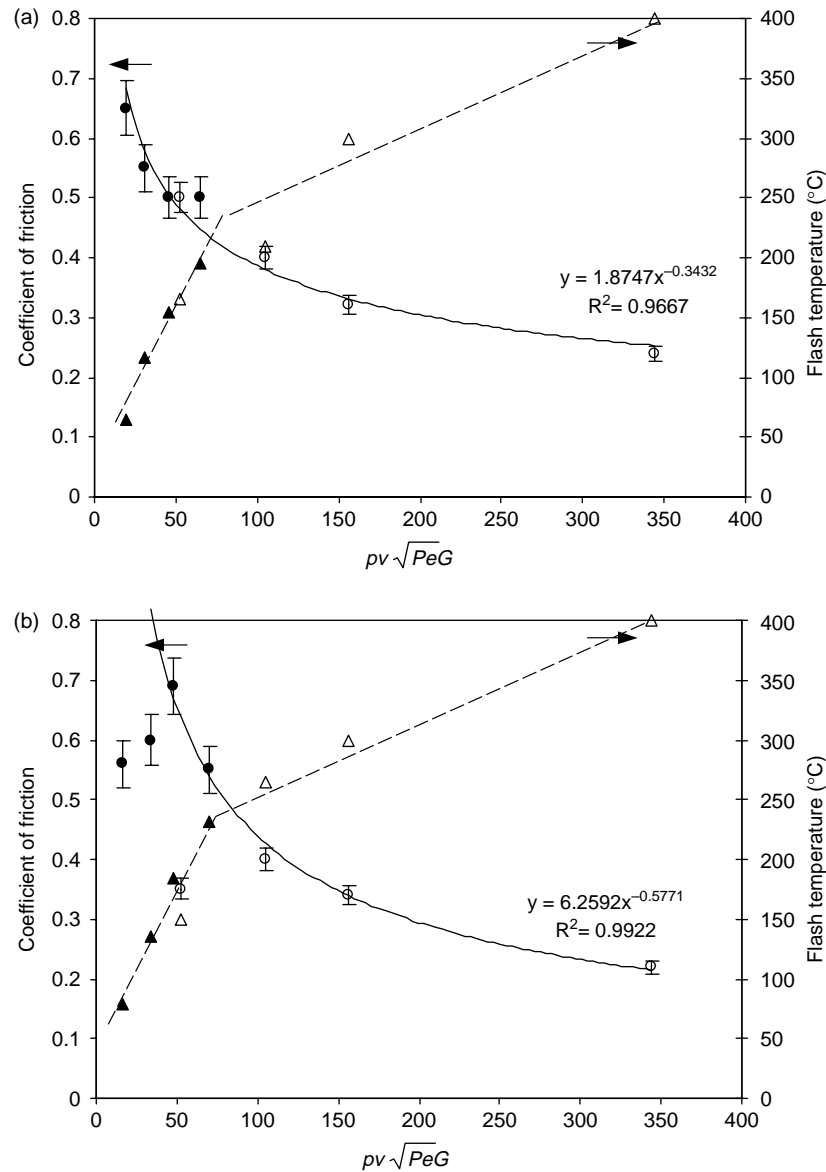


Fig. 11. Extrapolation of friction for (a) PA–Na and (b) PA–Mg (● small-scale friction, ▲ small-scale flash temperature, ○ large-scale friction, △ large-scale flash temperature).

Due to the transitions discussed before, which depend on either softening or melting, the wear rates on small-scale and large-scale tests show a different trend and cannot be compared. Even an artificial increase in sliding temperature on small-scale tests does not compensate for sliding conditions at high loads regarding wear. The estimation of real lifetime of polyamide components under high load conditions needs therefore specific tests as presently discussed.

## 5. Conclusions

Different influences of softening are observed on the friction and wear stability for either sodium or magnesium catalysed polyamides sliding against steel. Under low loads, where frictional heating not allows for melting, the sodium catalysed polyamides perform very high and unstable friction leading to a wavy surface pattern and no coherent transfer

film formation. Lower friction, lower wear and smooth sliding was observed for magnesium catalysed polyamides under low loads. This was correlated to the formation of a coherent transfer film. Melting under high loads, however, caused more severe wear for magnesium catalysed polyamide than for sodium catalysed polyamide. Transitions in the friction behaviour of oil-lubricated polyamides are not correlated to a specific transition temperature, but time-load related degradation of the polyamide bulk deteriorates the lubrication mechanisms.

Thermal analysis and Raman spectroscopy revealed that sodium catalysors rather promote the formation of an  $\alpha$  crystalline polyamide structure, while a  $\gamma$  crystalline structure with lower thermal resistance is favoured when using magnesium catalysors. After sliding, the  $\gamma$  structure slightly reverts into an  $\alpha$  structure, most likely on small-scale tests.

Extrapolation of tribological data between small-scale and large-scale testing is only possible in a limited regime. Small-scale sliding tests with controlled bulk temperatures are not able to compensate for large-scale tests under high load.

### Acknowledgements

The authors gratefully acknowledge Mr F. De Bruyne from Quadrant Engineering Plastics (Tielt, Belgium) for providing the test specimens and Mr R. Gillis for his technical assistance during large-scale testing.

### References

- [1] Rymuza Z. *Wear* 1996;199:187–96.
- [2] Li TQ, Zhang MQ, Song L, Zeng HM. *Polymer* 1999;40:4451–8.
- [3] Samyn P. *Tribol Lett*; in press.
- [4] Bark LS. *Wear* 1977;41:309–14.
- [5] Zhu J, Schweigen W. *KU Kunststoffe Plast Europe* 2001;91:55–6.
- [6] Samyn P, Van Schepdael L, Leendertz JS, Gerber A, Van Paepegem W, De Baets P, et al. *Tribol Int* 2006;39:796–811.
- [7] Van de Velde F, De Baets P. *Wear* 1997;209:106–14.
- [8] Samyn P, Quintelier J, Ost W, De Baets P, Schoukens G. *Polym Test* 2005;24:588–603.
- [9] Menges G. *Einführung in die Kunststoffverarbeitung*. Munchen: Carl Hanser Verlag; 1975.
- [10] Quadrant EPP. *General purpose plastic products: manual*, 2002.
- [11] Puffr R, Kubanek V, editors. *Lactam-based polyamide*, Vol. 1. Boca Raton: CRC Press; 1991.
- [12] Stehlicek J, Puffr R. *Macromol Chem* 1992;193:2539.
- [13] Kang SC, Chung DW. *Wear* 2000;239:244–50.
- [14] Blok H. *Wear* 1963;6:483–94.
- [15] Hooke CJ, Mao K, Walton D, Breeds AR, Kukureka SN. *Trans ASME J Tribol* 1993;115:119–24.
- [16] Bhushan B. *Principles and applications of tribology*. New York: Wiley-Interscience; 1999.
- [17] Jaeger CJ. *Proc R Soc* 1942;76:1107–21.
- [18] Lancaster JK. *J Lubr Technol* 1975;97:187–94.
- [19] Samyn P, Tuzolana T, Quintelier J. *STLE Annual Meeting 2006*, proceedings on CD.
- [20] Iwai T, Uchiyama Y, Shimosaka K, Takase K. *Wear* 2005;259:669–75.
- [21] Zsidai L, De Baets P, Samyn P, Kalacska G, Van Peteghem AP, Van Parys F. *Wear* 2002;253:637–88.
- [22] Yabe T, Takajo T, Kato S, Ueki F. *Tribol Trans* 2000;43:453–8.
- [23] Marchetti M, Meurisse HM, Vergne P, Sicre J, Durand M. *Tribol Lett* 2003;10:163–70.
- [24] Ferreira V, Depecker C, Laureyns J, Coulon G. *Polymer* 2004;45:6013–26.
- [25] Schmidt R, Fernandez MR, Pastor JM, Roda J. *Polymer* 1997;38:2067–75.
- [26] Murthy NS. *Polym Commun* 1991;32:301.
- [27] Rotter G, Ishida H. *J Polym Sci, Part B* 1992;30:489.
- [28] Lin L, Argon AS. *Macromolecules* 1994;27:6903–14.
- [29] Holmes DR, Bunn CW, Smith DJ. *J Polym Sci* 1955;17:159.
- [30] Arimoto H, Ishibashi M, Hirai M, Chatani Y. *J Polym Sci A* 1965;3:317.
- [31] Galeski A, Argon AS, Cohen RE. *Macromolecules* 1991;24:3945–52.
- [32] Jakes J, Krimm S. *Spectrochim Acta* 1971;27:35.
- [33] Vansanathan N, Salem DR. *J Polym Sci, Part B* 2001;39:536–47.
- [34] Penel-Pierron L, Depecker C, Seguela R, Lefebvre JM. *J Polym Sci, Part B* 2001;39:484–95.
- [35] Penel-Pierron L, Seguela R, Lefebvre JM, Miri V, Depecker C, Jutigny M, et al. *J Polym Sci, Part B* 2001;39:1224–36.
- [36] Maxfield MR, Christiani BR, Sanjeeva NM, Tuller H. *US Patent* 5,385,776, 1995.
- [37] Debowska M, Piglowski J, Slusarczyk C, Schmidt P, Rudzinska J, Suzuki T, et al. *Fibres Textiles* 2005;13(5):64–8.
- [38] Ramirez JMH, Colomban P, Bunsell A. *J Raman Spectrosc* 2004;35:1063–72.
- [39] Bessell TJ, Hull D, Shortall JB. *J Mater Sci* 1975;10:1127–36.
- [40] Bell JP, Dumbleton JH. *J Polym Sci, Part B* 1969;7:1033–57.
- [41] Ito M, Mizuochi K, Kanamoto T. *Polymer* 1998;39:4593–8.
- [42] Lin L, Argon AS. *Macromolecules* 1992;25:4011–24.
- [43] Stuart BH. *Tribol Int* 1998;31:687–93.
- [44] Miyasaka K, Ishikawa K. *J Poly Sci, Polym Phys* 1968;6:1317–29.
- [45] Czichos H. In: Lee LH, editor. *Polymer wear and its control*. ACS symposium series, Vol. 287. Washington: American Chemical Society; 1985.
- [46] Vermeulen M. *Wear* 1989;132:287–302.
- [47] Samyn P, De Baets P. *Wear* 2005;259:697–702.
- [48] Uetz H, Wiedemeyer J. *Tribologie der Polymere*. München-Vienna: Carl Hanser Verlag; 1985.
- [49] Pascoe MW, Tabor D. *Proc R Soc London* 1955;A235:210–24.
- [50] Yamaguchi Y. *Tribology of plastic materials*. Amsterdam: Elsevier; 1990.